

Kinetics of Bulk Lifetime Degradation in Float-Zone Silicon: Fast Activation and Annihilation of Grown-In Defects and the Role of Hydrogen versus Light

Daniel Hiller,* Vladimir P. Markevich, Joyce Ann T. de Guzman, Dirk König, Slawomir Prucnal, Wolfgang Bock, Jaakko Julin, Anthony R. Peaker, Daniel Macdonald, Nicholas E. Grant, and John D. Murphy

Float-zone (FZ) silicon often has grown-in defects that are thermally activated in a broad temperature window ($\approx 300\text{--}800^\circ\text{C}$). These defects cause efficient electron-hole pair recombination, which deteriorates the bulk minority carrier lifetime and thereby possible photovoltaic conversion efficiencies. Little is known so far about these defects which are possibly Si-vacancy/nitrogen-related (V_xN_y). Herein, it is shown that the defect activation takes place on sub-second time-scales, as does the destruction of the defects at higher temperatures. Complete defect annihilation, however, is not achieved until nitrogen impurities are effused from the wafer, as confirmed by secondary ion mass spectrometry. Hydrogenation experiments reveal the temporary and only partial passivation of recombination centers. In combination with deep-level transient spectroscopy, at least two possible defect states are revealed, only one of which interacts with H. With the help of density functional theory V_1N_1 -centers, which induce Si dangling bonds (DBs), are proposed as one possible defect candidate. Such DBs can be passivated by H. The associated formation energy, as well as their sensitivity to light-induced free carriers, is consistent with the experimental results. These results are anticipated to contribute to a deeper understanding of bulk-Si defects, which are pivotal for the mitigation of solar cell degradation processes.

1. Introduction


Float-zone (FZ) silicon is generally considered as a model material for high-efficiency Si photovoltaics (PV) and ubiquitous in research labs. Due to its high purity, with typical C and O concentrations $\leq 10^{16}\text{ cm}^{-3}$, and generally undetectable detrimental metal impurity concentrations, it exhibits high minority carrier bulk lifetimes and is not susceptible to phenomena such as impurity-related light-induced degradation at room temperature.^[1] FZ-Si was also used some years ago for high-volume manufacturing of solar cells^[2] with an at that time price-competitive fabrication method for PV-grade FZ.^[3,4] Apart from solar cells, FZ-Si is also used for radiation and particle detectors, where the minority carrier lifetime is also critical.^[5]

Recently, it was discovered that FZ-Si is not as ideal as commonly thought: Thermal treatments in a broad temperature range from about $450\text{--}700^\circ\text{C}$ were shown to dramatically degrade the bulk lifetime from

Dr. D. Hiller,^[†] Prof. D. Macdonald
Research School of Engineering
Australian National University (ANU)
Canberra, ACT 2601, Australia
E-mail: daniel.hiller@anu.edu.au

Dr. V. P. Markevich, J. A. T. de Guzman, Prof. A. R. Peaker
Photon Science Institute and School of Electrical and Electronic
Engineering
University of Manchester
Manchester M13 9PL, UK

Dr. D. König
Integrated Materials Design Centre (IMDC)
University of New South Wales (UNSW)
Sydney, NSW 2052, Australia

 The ORCID identification number(s) for the author(s) of this article can be found under <https://doi.org/10.1002/pssa.202000436>.

^[†]Present address: Institute of Semiconductors and Microsystems (IHM), Technische Universität Dresden, 01062 Dresden, Germany

DOI: 10.1002/pssa.202000436

Dr. D. König
Integrated Materials Design Lab (IMDL)
Australian National University (ANU)
Canberra, ACT 2601, Australia

Dr. S. Prucnal, Dr. J. Julin
Institute of Ion Beam Physics and Materials Research
Helmholtz-Zentrum Dresden-Rossendorf (HZDR)
01328 Dresden, Germany

Dr. W. Bock
Institute for Surface and Thin Film Analysis (IFOS)
67663 Kaiserslautern, Germany

Dr. J. Julin
Department of Physics
University of Jyväskylä
FI-40014 Jyväskylä, Finland

Dr. N. E. Grant, Prof. J. D. Murphy
School of Engineering
University of Warwick
Coventry CV4 7AL, UK

many milliseconds to $<100\ \mu\text{s}$.^[6–8] However, the bulk lifetime deteriorating defects can be **permanently annihilated** by high-temperature annealing **at $\geq 1000\ ^\circ\text{C}$** .^[6–8] Hydrogen (from H-rich dielectric coatings) was proposed to mitigate the effects of bulk lifetime degradation.^[6,9] We will demonstrate that the passivating effect of H is not permanent.

As the high-temperature mechanical stability of FZ-Si is greatly enhanced by adding N_2 gas to the atmosphere during crystal growth,^[10] the previous studies proposed Si-vacancies (V) and nitrogen (N) as constituents of V_xN_y -centers as the pertinent bulk-defect, and Mullins et al. provided striking evidence for this assumption.^[11] So far, only thermal treatments on long time-scales of ≥ 30 min were investigated. Here, we study FZ bulk lifetime degradation and defect annihilation as a function of annealing time over more than five orders of magnitude. In comparison to conventional tube furnace annealing (TFA), we also use annealing techniques such as rapid thermal annealing (RTA) or flash lamp annealing (FLA) and **reveal the critical role of above-bandgap light for the activation of the grown-in defects. The bulk lifetime degradation is found to occur on a sub-second timescale**, which renders it less probable to be associated with a diffusion-based defect formation process, but rather points toward a bond dissociation process generating the defects. Combined with results from hydrogenation, this finding strongly suggests that H-dissociation is involved in the activation of the V_xN_y -centers. In that respect, we study the role of H experimentally (lifetime measurements, deep-level transient spectroscopy (DLTS)) and theoretically (density functional theory [DFT] simulations).

Furthermore, it will be shown that the bulk lifetime can be **stabilized against subsequent thermal processing at significantly lower temperatures ($900\ ^\circ\text{C}$)** than the conventionally used 30–60 min annealing at around $1050\ ^\circ\text{C}$.^[12–16] The defect annihilation is **also found to be fast (sub-second timescale)**, although a fraction of the defects reappears during a subsequent degradation annealing. Together with N-quantification measurements by secondary ion mass spectrometry (SIMS), it is concluded that at high temperatures the V_xN_y -centers dissociate, **accompanied by an out-diffusion of nitrogen from the Si-wafer**. For short anneals, the effusion of N is insufficient and bears the potential for a reformation of defects.

For the purpose of bulk lifetime measurements that do not involve any processing at elevated temperatures (such as the

deposition of dielectrics with subsequent activation annealing), we use room-temperature superacid (SA)-passivation of the Si-surfaces by bis(trifluoromethane)sulfonimide (TFSI)^[17] dissolved in hexane.^[18] This passivation procedure allows for reliable and reproducible surface passivation with typical surface recombination velocities $S_{\text{eff}} < 1\ \text{cm s}^{-1}$.^[16,18] Such a passivation quality is sufficient to identify the measured effective lifetime (τ_{eff}) with the bulk lifetime (τ_{bulk}) and, as it is performed at room temperature, it does not affect the bulk lifetime under investigation.

2. Results

2.1. SA-Passivation Pretreatments

Grant et al. demonstrated that the chemical pretreatments before the SA treatment are decisive for a near-perfect surface passivation.^[16] Whereas, an H-terminated Si surface [from a hydrofluoric acid (HF)-dip] is a general requirement of the SA-passivation technique,^[17] preceding cleaning or etching steps can have a huge influence on the passivation quality.^[19] For instance, it was shown that etching of the surface with tetramethylammonium hydroxide (TMAH) combined with an RCA-2 cleaning results in maximum lifetimes^[16] and this procedure was also adopted by others.^[18,20] In contrast, a simple HF-dip without any etching/cleaning or a RCA-1 cleaning with HF-dip was shown to result in ≈ 4 or 40-times lower lifetimes, respectively, which is not related to the surface roughness of mirror-polished wafers.^[16]

To clarify the impact of chemical pretreatments on the SA-passivation quality on the $\approx 280\ \mu\text{m}$ thick saw-damage etched $2\ \Omega\ \text{cm}$ n-type FZ-Si wafers used here, eight different combinations of TMAH-etching, RCA-1, RCA-2, and HF-HCl-dips were tested, as specified in **Table 1**. The measured effective minority carrier lifetimes (τ_{eff}) as a function of minority carrier density as well as uncalibrated photoluminescence (PL) images are shown in **Figure 1**. Apparently, the SA-passivation on saw-damage etched wafers is not very sensitive to the pretreatment procedure. A maximum lifetime of $\approx 6.7\ \text{ms}$ at $10^{15}\ \text{cm}^{-3}$ injection is measured for four different procedures (C, F, G, H) and even just a simple HF-dip alone (A) results in a remarkable 6.4 ms. Notably, we cannot reproduce the detrimental impact of RCA-1 cleaning

Table 1. Chemical surface pretreatments before SA passivation. Before step 1, all as-cut wafers were initially RCA-cleaned, saw-damage etched (25% TMAH, $80\ ^\circ\text{C}$, 20 min), RCA-cleaned again, and annealed in O_2 at $900\ ^\circ\text{C}$ for 30 min to mimic a typical annealing. Between each etching/cleaning step, the samples were thoroughly rinsed in DI-water. However, after the final dip in HF-HCl-solution, they were immersed directly in SA-solution without DI-water rinsing.

SA pretreat-ment	Step 1	Step 2	Step 3	Step 4	Step 5	Step 6	Step 7
A	HF-HCl-dip ($\approx 5\%$)	–	–	–	–	–	–
B	HF ($\approx 5\%$)	TMAH (10 min)	HF-HCl-dip ($\approx 1\%$)	–	–	–	–
C	HF ($\approx 5\%$)	RCA-1	HF-HCl-dip ($\approx 1\%$)	–	–	–	–
D	HF ($\approx 5\%$)	RCA-2	HF-HCl-dip ($\approx 1\%$)	–	–	–	–
E	HF ($\approx 5\%$)	TMAH (10 min)	HF-HCl-dip ($\approx 1\%$)	RCA-1	HF-HCl-dip ($\approx 1\%$)	–	–
F	HF ($\approx 5\%$)	TMAH (10 min)	HF-HCl-dip ($\approx 1\%$)	RCA-2	HF-HCl-dip ($\approx 1\%$)	–	–
G	HF ($\approx 5\%$)	TMAH (10 min)	HF-HCl-dip ($\approx 1\%$)	RCA-1	HF-HCl-dip ($\approx 1\%$)	RCA-2	HF-HCl-dip ($\approx 1\%$)
H	HF ($\approx 5\%$)	TMAH (10 min)	HF-HCl-dip ($\approx 1\%$)	RCA-2	HF-HCl-dip ($\approx 1\%$)	RCA-1	HF-HCl-dip ($\approx 1\%$)

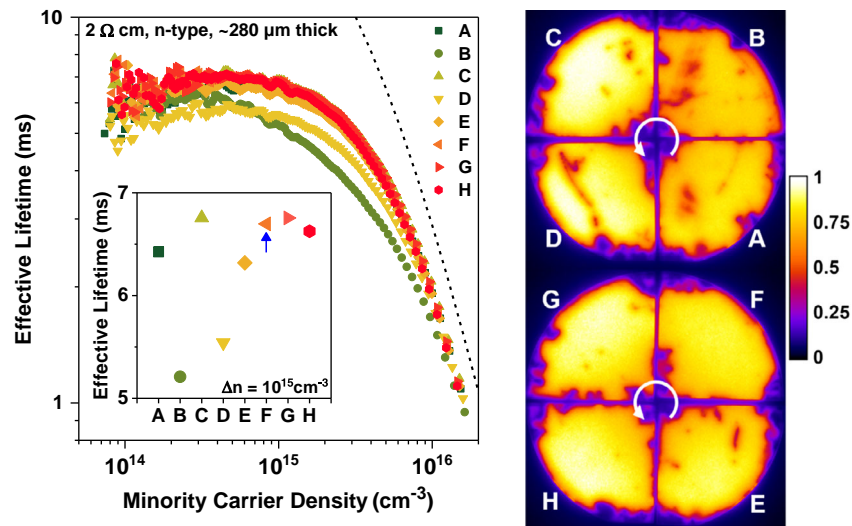


Figure 1. Injection-dependent effective lifetimes of FZ-Si subjected to the chemical pretreatments specified in Table 1 before SA-passivation. The black dashed line represents the intrinsic lifetime limit according to refs. [21]. The inset shows the effective lifetimes at an excess minority carrier density of $1 \times 10^{15} \text{ cm}^{-3}$. The arrow indicates procedure F, which will be used throughout this study. On the right-hand side, uncalibrated PL images of the samples are shown to highlight spatial nonuniformities of the surface passivation (scale bar in relative counts).

for saw-damage etched surfaces that was found for polished wafers.^[16] PL imaging reveals that all procedures involving TMAH-etching and RCA-1/2 cleaning(s), i.e., procedures E–H, generally provide less surface defects (dark spots). However, in absence of detailed statistics, sample-to-sample fluctuations cannot be excluded and therefore this result should not be overstated. As procedure F (HF, TMAH, HF, RCA-2, HF) results in a very good passivation, is compatible with general sample preparation, and is also in accordance with literature,^[16,18,20] it will be used throughout this study.

2.2. Temperature- and Time-Dependence of Bulk Lifetime Degradation

Initially, we attempt to reproduce the annealing temperature dependence of the FZ-Si bulk lifetime for 30 min TFA. Here, O_2 atmosphere is used for all annealing processes, though it was recently demonstrated that the bulk lifetime degradation is not sensitive to the atmosphere (i.e., O_2 , N_2 , Ar) over the range of 450–700 °C.^[11] As shown in Figure 2a (blue squares), the bulk lifetime remains on a high level of several milliseconds until 400 °C, drops suddenly when reaching 500 °C, remains on average at $\approx 46 \mu\text{s}$ until 700 °C and partially or fully recovers to initial lifetime values for 800/900 °C, respectively. For a batch of samples that were annealed previously at 1100 °C for 30 min, the grown-in defects of FZ-Si appear to be annihilated and the minority carrier lifetime is consequently insensitive to any subsequent thermal treatments (cf. gray open squares in Figure 2a). This is exactly the behavior outlined in refs. [6–8].

When reducing the annealing dwell time to only 30 s using RTA (bright green circles in Figure 2a), two observations can be made: The onset of severe bulk lifetime degradation is shifted to lower temperatures (400 °C), whereas the lifetime recovery remains at 900 °C. The bulk lifetimes in the degraded state

are on average $\approx 33 \mu\text{s}$, i.e., almost identical to the 60 times longer annealed TFA samples.

Next, FLA is used to reduce the total annealing time even further with flash pulse durations of only 20 ms (single-side flashes without using any lamp preheating). Bulk lifetime degradation is found to occur from a peak surface temperature of 600 °C onward, without any recovery for 900 °C (cf. red triangles in Figure 2a). Depending on the energy density emitted by the Xe-flash lamp, the wafer surface is heated to the desired temperature (derived from surface melting experiments and simulations) and decays immediately after the pulse to an equilibrium temperature, which is quite homogeneously distributed over the wafer thickness.^[22] This equilibrium temperature increases with pulse duration, and 20 ms, the maximum of typical FLA systems, allows for minimal peak-to-equilibrium differences.^[22] The temperature difference between front- and backside is expected to be $< 100 \text{ K}$. This temperature gradient over the wafer thickness might explain the temperature shifts of lifetime degradation compared with RTA and TFA. In any case, the FLA-experiment unequivocally proves that even sub-second heat treatments at the borderline to thermal nonequilibrium dramatically degrade the bulk lifetime.

The RTA processes used here have standard heating/cooling ramp rates of $\pm 20 \text{ K s}^{-1}$ and therefore keep the wafer in thermal equilibrium even for reduced dwell times. Figure 2b shows that the bulk lifetimes can be fully degraded at 550 °C even by a 1 s short RTA and no fundamental changes in τ_{bulk} occur for longer anneals. Also, varying the heating/cooling ramp rates of the RTA (± 2 to $\pm 75 \text{ K s}^{-1}$) does not change the bulk lifetimes, as clear from Figure 2c (bright green circles).

Hence, it is concluded that all thermal processes in the critical temperature window of ≈ 400 –800 °C (in thermal equilibrium) are very detrimental for the bulk lifetimes of FZ-Si and resulting solar-cell efficiencies, irrespective of annealing technology, dwell time or ramp rates. Furthermore, the circumstance that the grown-in defects are activated on very fast timescales has

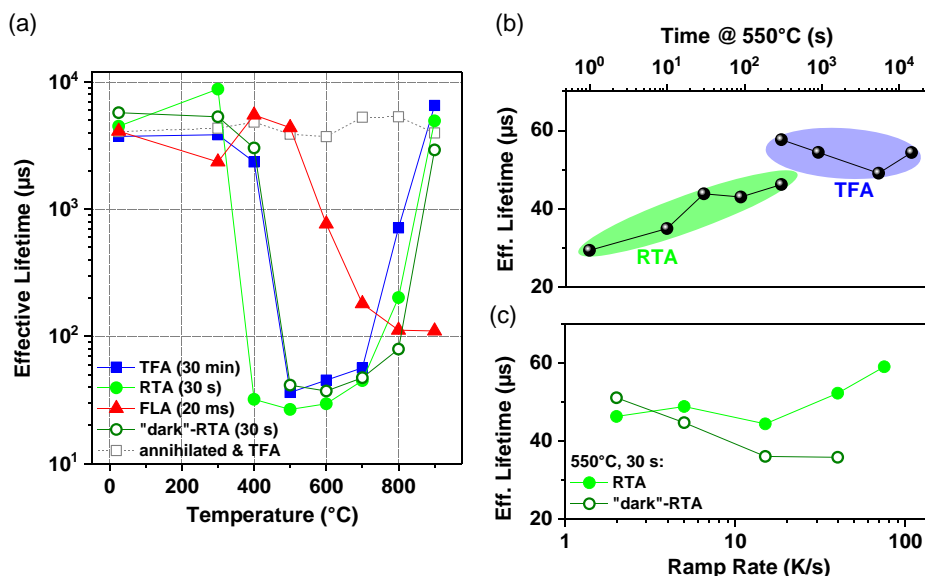


Figure 2. a) Bulk lifetimes of SA-passivated 2 Ω cm n-type FZ Si (at $\Delta n = 10^{15} \text{ cm}^{-3}$) for thermal treatments using various technologies with durations ranging over more than four orders of magnitude. FLA-temperatures refer to the peak surface temperature. Note, that FLA-samples were exposed to a single-side flash, which inevitably results in a temperature gradient over the wafer thickness. For experimental details about each annealing method and its temperature calibration, see Section 5. b) Bulk lifetime degradation as a function of annealing dwell time at 550 °C (RTA with $\pm 20 \text{ K s}^{-1}$ ramps). c) Bulk lifetime degradation versus heating/cooling ramp rate in the RTA at 550 °C with 30 s dwell time.

important implications for the possible defect structures and their formation process.

2.3. Bulk Lifetime Degradation and Annihilation: The Role of Light

The major difference between the TFA and RTA processes used here is the electromagnetic spectrum which the FZ-Si sample is subjected to during the thermal treatment. In a resistively heated tube furnace, there is mainly infrared radiation with only a diminutive emission shoulder in the spectral range above the Si bandgap (1.12 eV) for the highest temperatures, according to Planck's law of black-body radiation. In contrast, RTA uses halogen lamps for heating, which emit a significant fraction of their light with energies above the Si bandgap. It could be argued that the huge flux of visible photons during a high-temperature RTA process and the resulting photogenerated free carrier density can interfere with the formation and annihilation of the grown-in defects. Therefore, we sandwiched FZ-Si samples between two RCA-cleaned 400 μm thick dummy Si wafers in the RTA chamber to absorb all above-bandgap light without significantly compromising the temperatures. This procedure is labeled "dark"-RTA.

From Figure 2a, it can be seen that the degradation behavior of the "dark"-RTA samples (open dark green circles) is virtually identical to the TFA-samples, i.e., still high bulk lifetimes for 400 °C, in contrast to ("bright")-RTA. On the other hand, a complete high-temperature lifetime recovery requires also 900 °C, whereas at 800 °C the sample is still significantly degraded ($< 100 \mu\text{s}$). Arguably, a significant contribution of visible light during the thermal processing (i.e., for "bright"-RTA) reduces the thermal energy required for the formation of the bulk lifetime degrading defects,

but it does not influence their annihilation. It is worth pointing out that due to the slow ramp rates of $\pm 20 \text{ K s}^{-1}$ and the comparatively long 30 s dwell time, the "dark"-RTA samples are well in thermal equilibrium, although the sandwich wafers might slightly delay the ramps. Figure 2c corroborates that a variation of the heating/cooling ramp rate over more than one order of magnitude has only minute influence on the degradation by "dark"-RTA as compared with the annealing temperature.

2.4. Temperature- and Time-Dependence of Defect Annihilation

It has previously been shown that the thermally activated bulk lifetime degrading defects can be permanently annihilated by annealing at $\geq 1000 \text{ °C}$ for 30–60 min.^[6,7] However, the data shown in Figure 2a demonstrate that already at 800 °C a partial lifetime recovery can be achieved for long annealing times. To clarify the minimum thermal requirements for defect annihilation, the temperature range $\geq 800 \text{ °C}$ was investigated in detail for annealing dwell times from 1 min to 2 h using RTA and TFA, as well as FLA up to the melting temperature of Si. The results are presented in Figure 3.

For TFA, a medium-high bulk lifetime of $\approx 4 \text{ ms}$ is observed for $\geq 1 \text{ h}$ at 800 °C, whereas shorter times are completely insufficient (blue squares). At 900 °C, maximum bulk lifetimes of $\approx 8 \text{ ms}$ are achieved for 15 min (green circles), whereas 1 min TFA just reaches an intermediate lifetime level—in contrast to 1 min RTA, which also results in a lifetime of $\approx 8 \text{ ms}$ (open green circle). At 1000 and 1100 °C, the defect annihilation is already completed after 1 min dwell time (orange and red triangles). Interestingly, the lifetimes drop again for $\geq 1 \text{ h}$ —just slightly for 1000 °C, but significant for 1100 °C. All TFA processes were conducted in pure O₂ atmosphere in a quartz glass tube

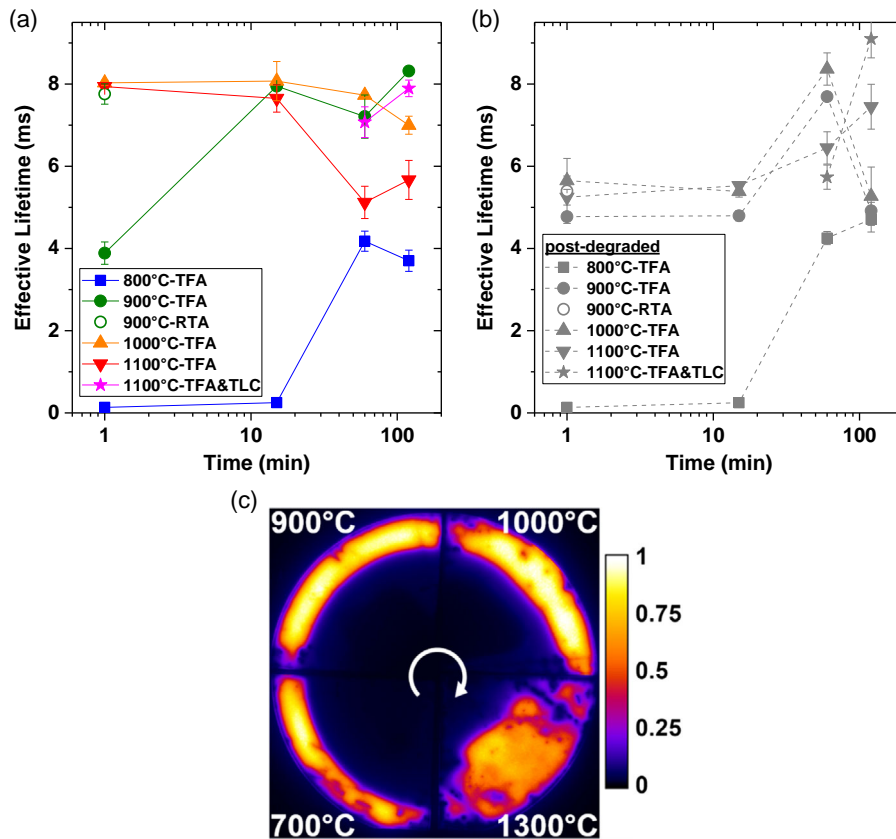


Figure 3. a) Bulk lifetimes of SA-passivated 2 Ω cm n-type FZ Si (at $\Delta n = 10^{15} \text{ cm}^{-3}$) for various defect annihilation processes. b) Lifetimes of the same samples after an additional degradation annealing to test for possible reformation of bulk defects. c) Uncalibrated PL images of degraded samples with annihilation attempted using 20 ms FLA at the indicated temperatures (scale bar in relative counts).

that was cleaned by a high-temperature process using *trans*-1,2-dichloroethylene (TLC) each time before processing a batch of samples. Nevertheless, we observe a loss of ≈ 2 ms in bulk lifetime for long, high-temperature annealing, which can only be avoided by replacing the oxidation in pure O_2 by a TLC-oxidation, i.e., an oxidation process in which a part of gas flow is bubbled through TLC (cf. pink asterisks in Figure 3a). This result underpins the utmost importance of high cleanliness and high purity for the defect annihilation in FZ-Si by long high-temperature annealing. In contrast, shorter or lower temperature annihilations are significantly less prone to potential contaminations.

When the same samples of Figure 3a are rinsed to remove their SA-passivation, followed by a full RCA-clean, thermal degradation in the 600 °C range (30 min, TFA), and finally SA repassivated, a bulk lifetime loss of ≈ 2 –3 ms down from the ≈ 8 ms level is observed for the 1 min and 15 min processes, but not for 60 min (see Figure 3b). Hence, the potential for annealing time reductions might not be as high as the potential for temperature reductions toward the ≈ 900 °C range (for >15 min).

We note that these conditions fall approximately within the process temperature windows of homojunction diffusion and of various poly-Si-based passivating contact technologies (i.e., so-called poly Si on oxide (POLO)), tunnel oxide passivated contacts (TOPCon), or polycrystalline silicon on interfacial oxide (Poly-Ox), etc.^[23–26] Thus, high-temperature pretreatments to

stabilize the bulk lifetime might be avoided when such fabrication steps are used. However, to achieve maximum effective lifetimes (up to >100 ms), a high-temperature pretreatment prior to TOPCon passivation, for example, still appears beneficial.^[15,27]

In Figure 3c, the effect of high-temperature FLA of bulk lifetime degraded samples (via 400 °C, 1 min lamp preheating) is shown. The high-lifetime ring at the wafer edge, where the concentration of vacancies is lower,^[11] increases slightly for a 1000 °C-flash and grows toward the wafer center for a 1300 °C-flash. The extended high-lifetime area (yellow–orange region in Figure 3c) reaches 1.75 ms as measured by photoconductance decay. Further increasing the energy density of a single flash up to the melting point of Si (i.e., surface temperature ≥ 1414 °C) significantly deteriorates the bulk lifetime, despite a thorough removal of the molten layer by extended TMAH-etching before SA-passivation (≈ 25 μm per side). Also, adding a second and a third 1300 °C flash leads to <1 ms bulk lifetimes. Although it is instructive to observe partial defect annihilation on sub-second timescales, it appears that FLA cannot be used to entirely stabilize the bulk lifetime in FZ-Si.

2.5. Arrhenius Plots of Bulk Lifetimes

It is clear from Figure 2a that both the activation and the annihilation of the bulk lifetime degrading defects are rather abrupt

processes that occur within $\approx 100^\circ\text{C}$ -intervals. Hence, we subdivided the temperature intervals for TFA (here 60 min) and RTA (30 s) in the critical temperature range into steps as small as 17°C to extract estimates for the formation energies via Arrhenius plots. The results are shown in **Figure 4a**. For TFA, the linear fit reveals a defect formation energy of $2.0 \pm 0.3\text{ eV}$

(error refers to deviation by residual squares in fitting procedure), which is reduced to $1.2 \pm 0.1\text{ eV}$ for RTA. The 0.8 eV lower formation energy is attributed to the additional component of above-bandgap light, which apparently supports the defect formation. In **Figure 4b**, it is demonstrated how abrupt and temperature-sensitive the degradation is for 60 min TFA:

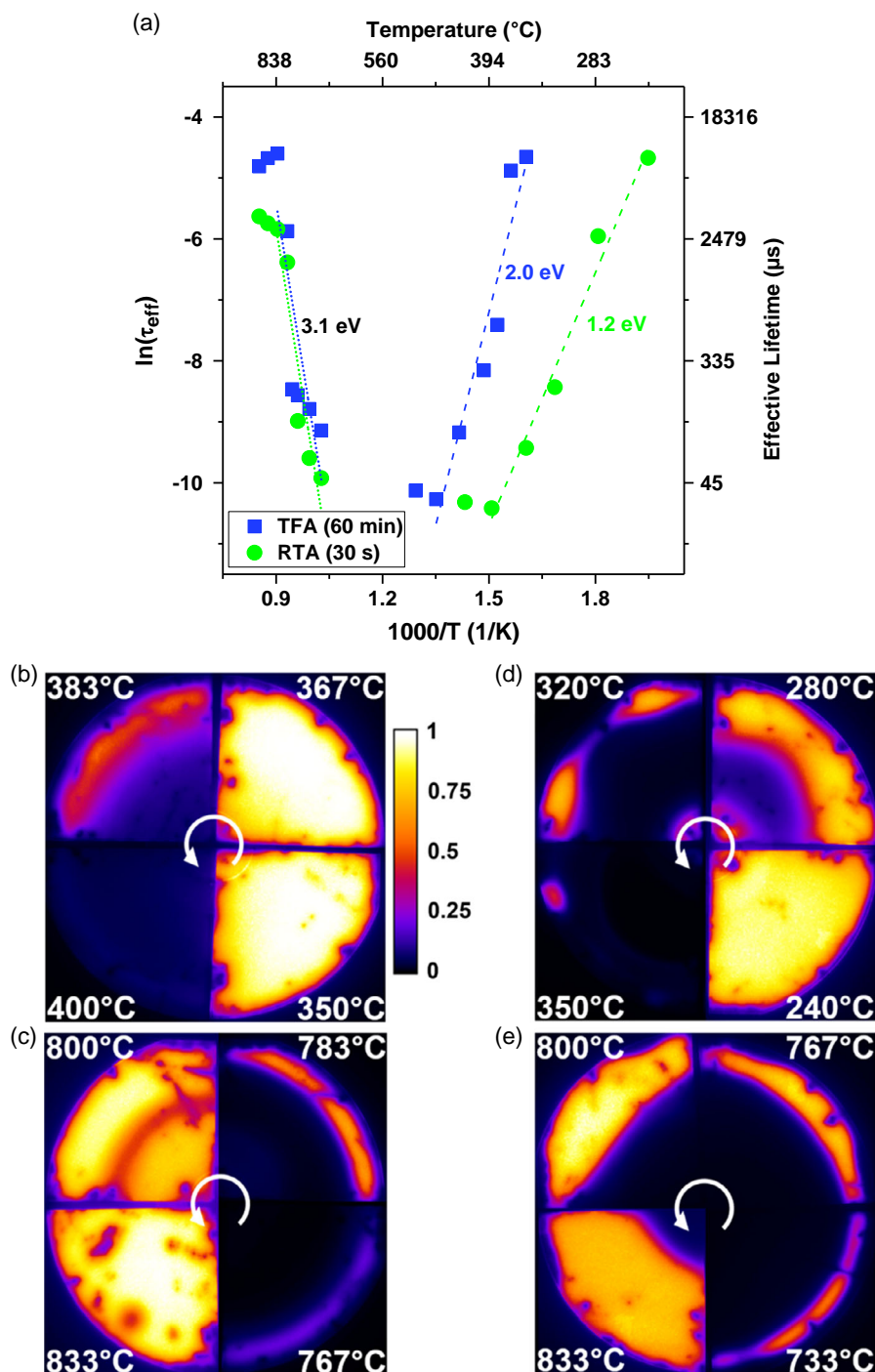


Figure 4. a) Arrhenius plot of the bulk lifetimes of the degradation and defect annihilation process with estimated formation energies extracted by linear fits. b,c) Uncalibrated PL images of 60 min TFA samples that visualize the spatial evolution of the activation/annihilation of bulk lifetime degrading defects, as well as the abruptness of the respective process (scale bar in relative counts). d,e) The corresponding PL images of the 30 s RTA samples.

At 367 °C, the sample is essentially undegraded, although maybe a slight reduction in bulk lifetime in the wafer middle is present when compared with 350 °C. However, for 383 °C, the whole center of the wafer is fully degraded. For RTA degradation (30 s), the critical temperature is between 240 and 280 °C, as shown Figure 4 d (a small difference compared with the data in Figure 2a is attributed to possible short temperature overshoots during ramp up). The 280 °C-RTA sample demonstrates clearly that the lifetime degradation starts in a zone that is equally spaced from the center and the edge of the wafer.

The same abruptness and temperature-sensitivity is observed for the annihilation of the defects and the recovery of bulk lifetimes, as shown in Figure 4c. From 767 to 783 °C, just the wafer edge regains some PL-emission activity, whereas the center remains dark. Just 17 °C more (i.e., 800 °C) is sufficient to largely recover the bulk lifetime. Interestingly, it can be seen that the high-lifetime zones grow from two directions, i.e., from the wafer edge toward the center and vice versa, similar to the degradation pattern of the 280 °C-RTA sample. The low-lifetime ring finally vanishes for 833 °C. Similar observations are made for RTA (30 s), where the lifetime recovery grows solely from the wafer edge toward the center, starting from 767 °C and leaving only an ≈ 15 mm radius zone in the middle of the wafer defective for 833 °C, cf. Figure 4e (diminishing for higher temperatures, not shown). The corresponding linear fits in the Arrhenius plot reveal equal formation energies of the defect annihilation of 3.1 ± 1.0 eV for TFA and 3.1 ± 0.7 eV for RTA, respectively. Please note that the use of τ_{eff} data in Arrhenius plots rather than degradation/recovery rates can be considered problematic. However, due to the pronounced temperature sensitivity and marginal time dependence of the processes, an extraction of rates is unreliable. Future experiments will have to subdivide the temperature intervals in even finer steps combined with a time variation to corroborate the data.

2.6. Bulk Lifetime Degradation and Annihilation: The Role of Hydrogen

Rougieux et al. demonstrated that the detrimental, lifetime-reducing impact of the bulk defects can be mitigated to some extent when wafers are thermally processed with hydrogen-containing capping layers such as atomic layer deposition (ALD)- Al_2O_3 or (preferably) plasma enhanced chemical vapor deposition (PECVD)- $\text{SiN}_x\text{:H}$.^[6] Very recently, it was shown that the bulk lifetime of a degraded sample can be improved by one order of magnitude by an annealing of the wafer with a PECVD- $\text{SiN}_x\text{:H}$ layer.^[9]

In Figure 5a, the bulk lifetime degradation and defect annihilation for 30 min TFA in the presence of 105 nm PECVD- $\text{SiN}_x\text{:H}$ (blue open squares) and 20 nm ALD- Al_2O_3 (purple squares) is shown. All anneals in this section are done in N_2 -atmosphere rather than O_2 to prevent any reactions between hydrogen and oxygen at elevated temperatures. The onset of degradation occurs for 500 °C, same as for the uncoated samples (cf. Figure 2a), but the lowest lifetimes at 600 °C are ≈ 200 –300 μs (in contrast to < 50 μs uncoated). The bulk lifetimes (measured here after stripping the coatings and SA-passivation, unlike ref. [6]) of both

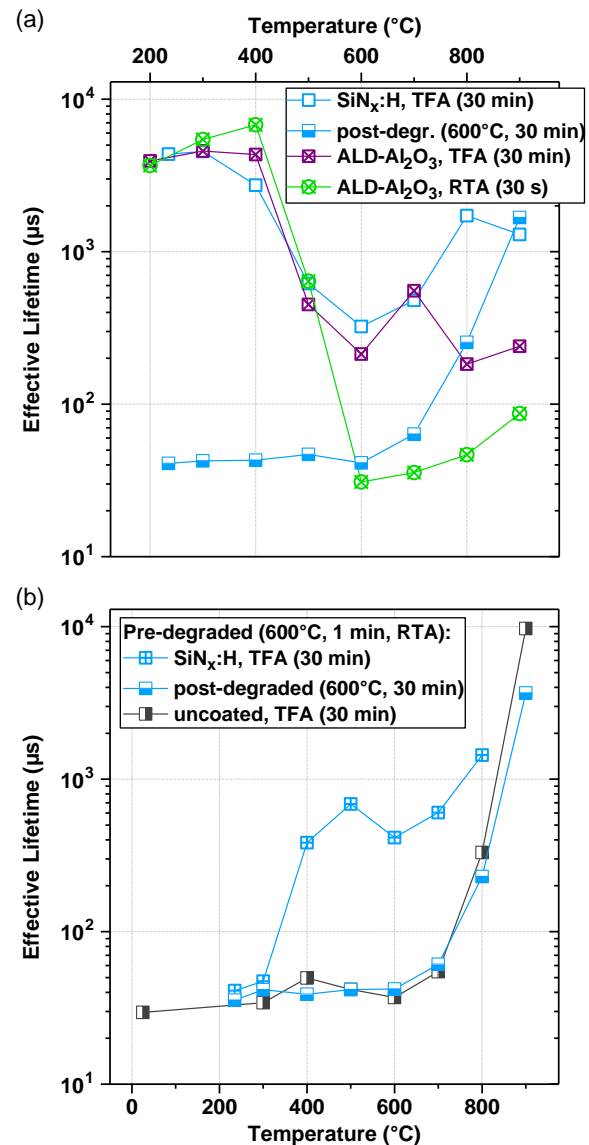


Figure 5. a) Bulk lifetimes of SA-passivated n-type FZ Si (at $\Delta n = 10^{15} \text{ cm}^{-3}$) annealed with H-rich dielectric coatings. b) A similar experiment with samples that were lifetime-degraded before deposition of silicon nitride and annealing. Half-filled squares in both graphs indicate samples that were cleaned and subjected to an additional degradation annealing to demonstrate the instability of defect hydrogenation.

dielectrics in the fully degraded state do not differ significantly, despite a factor of ≈ 30 lower amount of H in Al_2O_3 ($\approx 7 \times 10^{15} \text{ H cm}^{-2}$ with $[\text{H}] \approx 2.9 \text{ at\%}$ at 200 $^{\circ}\text{C}$ -ALD)^[28–30] versus $\text{SiN}_x\text{:H}$ ($\approx 2.11 \times 10^{17} \text{ H cm}^{-2}$ with $[\text{H}] = 20.5 \text{ at\%}$ as measured by elastic recoil detection analysis (ERDA)). Note that ERDA quantifies the total amount of H in the dielectric film irrespective of different bond configurations, and differences in these configurations could affect the concentration of hydrogen which has entered the Si bulk. Even an only 5 nm thick ALD- Al_2O_3 layer (not shown) is capable to maintain ≈ 200 μs bulk lifetime after 600 $^{\circ}\text{C}$, 30 min TFA. Hence, neither the H-providing material nor (over a broad range) the H-concentration

in that material play a role in mitigating the bulk lifetime degradation. In addition, we cannot see any influence of other impurities in the dielectrics on the bulk lifetime: Although ALD- Al_2O_3 is generally considered rather clean (except for typically $\lesssim 0.3$ at% carbon),^[29,30] we detected slightly more impurities in the PECVD- $\text{SiN}_x\text{:H}$ (0.6 at% carbon, 0.6 at% fluorine).

If Al_2O_3 -coated FZ-Si is RTA-annealed for 30 s, the degradation at 600 °C does not differ from uncoated samples (≈ 30 μs) and does also not recover at high temperatures (cf. green data points in Figure 5a). Even an only 1 s short RTA (550 °C) of Al_2O_3 -coated samples still degrades the bulk lifetime to the < 100 μs range. Consequently, on the assumption that the hydrogen content in the dielectric gives a reliable estimation of H in the bulk, H hardly counteracts bulk lifetime degradation for RTA, which again underlines the role of above-bandgap light.

Note, that for none of the processes described here blistering of the dielectric films was observed due to outgassing hydrogen, which would have compromised the spatial homogeneity of the H-source.

Most importantly, we show that hydrogen does not provide a permanent deactivation of the bulk lifetime degrading defects. The formerly $\text{SiN}_x\text{:H}$ -coated samples were rinsed to remove their SA-passivation, followed by a full RCA-clean, and thermally degraded again (600 °C, 30 min, TFA). All low- and medium-temperature-processed samples become fully degraded with an average lifetime of 43 μs until thermal annihilation sets in for ≥ 800 °C (cf. blue half-filled squares in Figure 5a).

The bulk lifetime development of degraded uncoated samples (gray half-filled squares) and pre-degraded $\text{SiN}_x\text{:H}$ -coated samples (blue squares) that were subjected to 30 min TFA over the whole temperature range is shown in Figure 5b. Starting from 400 °C, the $\text{SiN}_x\text{:H}$ -coated samples have more than one order of magnitude higher lifetimes than the uncoated samples, although the absolute values do not exceed 1 ms, unless additionally thermal defect annihilation comes into play for ≥ 800 °C. Again, rinsing, cleaning and thermally degrading (600 °C, 30 min, TFA) the formerly $\text{SiN}_x\text{:H}$ -coated samples makes their temperature evolution identical to that of the degraded uncoated samples. In other words, FZ-Si has no memory for H-induced thermal mitigations of bulk lifetime degradation. Hydrogen does only provide a partial prevention of degradation during thermal processing as long as an H-rich dielectric is present on its surface.

As hydrogen is a volatile impurity in the dielectric coatings used here, it is expected to diffuse not only into the wafer but also out of the layer into the ambient during annealing. Accordingly, we expect the H-source to deplete with time, and together with it the bulk lifetime will decrease. **Figure 6** shows the time evolution of $\text{SiN}_x\text{:H}$ -coated, degraded $\text{SiN}_x\text{:H}$ -coated and Al_2O_3 -coated FZ-Si during 600 °C TFA. Overall, both pristine dielectric-coated sample sets are continuously degrading in lifetime as a function of time. The pre-degraded (600 °C, 1 min, RTA) $\text{SiN}_x\text{:H}$ -coated samples reach the typical H-related intermediate lifetime level within only 5 min at 600 °C and then degrade similarly. The lifetime evolution can be fitted by exponential decay functions with time constants of ≈ 40 min for $\text{SiN}_x\text{:H}$ versus ≈ 13 min for Al_2O_3 . Possibly, the $\approx 30\times$ higher amount of H in $\text{SiN}_x\text{:H}$ compared with ALD- Al_2O_3 delays the lifetime degradation induced by H-effusion.

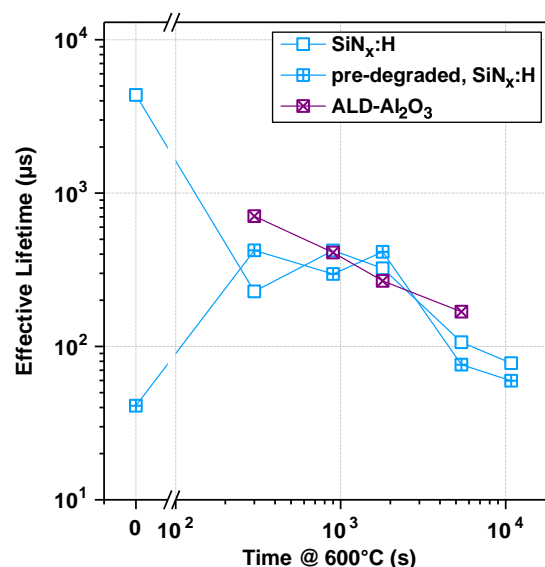


Figure 6. Bulk lifetimes of SA-passivated n-type FZ Si (at $\Delta n = 10^{15} \text{ cm}^{-3}$) annealed with H-rich dielectric coatings as a function of annealing time at 600 °C (TFA).

2.7. Nitrogen Quantification

SIMS measurements in the center and at the edge of a FZ-Si wafer demonstrated equal N-concentrations,^[6] whereas vacancy decoration experiments using Ni and DLTS confirmed that the origin of the high-lifetime wafer edge is related to a lower concentration of Si-vacancies at the edge compared with the center.^[11] Here, the N-concentrations were analyzed using dynamic SIMS in a depth of $\approx 5\text{--}25$ μm and following a procedure proposed for light trace impurities.^[31]

In the unprocessed state, i.e., without any annealing, $[N] = (4.7 \pm 0.9) \times 10^{14} \text{ cm}^{-3}$ is measured, which is a very typical value for FZ-Si that is not specifically fabricated to be N-lean.^[6–8,11] A sample that was defect-annihilated by a long high-temperature anneal (1 h TLC-oxidation at 1100 °C) does not have a N-concentration above the detection limit, which was estimated here to be $5 \times 10^{13} \text{ cm}^{-3}$. Hence, we prove that N effuses from FZ-Si during a conventional defect-annihilation anneal, which implies that the defects which degrade the bulk lifetime are dissolved via removal of at least one of their constituents. However, in a FZ-Si sample that was defect-annihilated by a short medium-temperature anneal (1 min RTA at 900 °C) a residual amount of $\approx [N] = (0.7 \pm 0.1) \times 10^{14} \text{ cm}^{-3}$ is still detectable, which casts the aforementioned assumption into doubt that defect annihilation is equal to a complete N-effusion from the wafer as a whole. Comparing with Figure 3a, it is clear that the 1 h-1100 °C sample and the 1 min-900 °C sample have both near-maximum bulk lifetimes of > 7 ms, which is incompatible with a significant defect concentration. This points toward a temperature-induced dissociation reaction (both TFA and RTA sample) followed by the slow out-diffusion of N (only TFA sample). In Section 3.2, we provide a comprehensive model to explain these observations in detail. The SIMS results and bulk lifetimes are summarized in Table 2.

Table 2. Nitrogen concentrations quantified by SIMS and bulk lifetimes of FZ-Si subjected to different thermal treatments.

Annealing method	Temperature [°C]	Dwell time [min]	N-concentration [10^{14} cm^{-3}]	τ_{eff} at $\Delta n = 10^{15} \text{ cm}^{-3}$ [ms]
Not annealed	N/A	N/A	4.7 ± 0.9	4.49
TFA	1100	60	< 0.5	7.07
RTA	900	1	0.7 ± 0.1	7.76

For carbon and oxygen, the concentrations are very close to or below the detection limits of $\approx 2 \times 10^{15}$ and $\approx 1 \times 10^{16} \text{ cm}^{-3}$, respectively, and in accordance with the wafer manufacturer's specifications. Therefore, no changes can be detected in the concentrations of these two light impurities as a function of annihilation annealing.

2.8. DLTS

Figure 7 shows DLTS spectra of samples subjected to different anneals with and without $\text{SiN}_x\text{:H}$ coating, as specified in Table 3. The thermally unprocessed sample I does not show any electron traps in the DLTS spectra, whereas in the other samples five different peaks were observed. However, only two of these peaks appear to be correlated with the bulk lifetimes. Samples II and III, which were subjected to a hydrogenation as a last process step, have both intermediate bulk lifetimes ($\approx 300 \mu\text{s}$), but they only have peak E_4 in common (highlighted in red) that has a corresponding electron activation energy of $0.336 \pm 0.003 \text{ eV}$. Samples IV and V are both fully τ_{bulk} -degraded ($\approx 40 \mu\text{s}$) as they were either never hydrogenated (IV) or H was effused by annealing after stripping the $\text{SiN}_x\text{:H}$ layer (V). In these two samples,

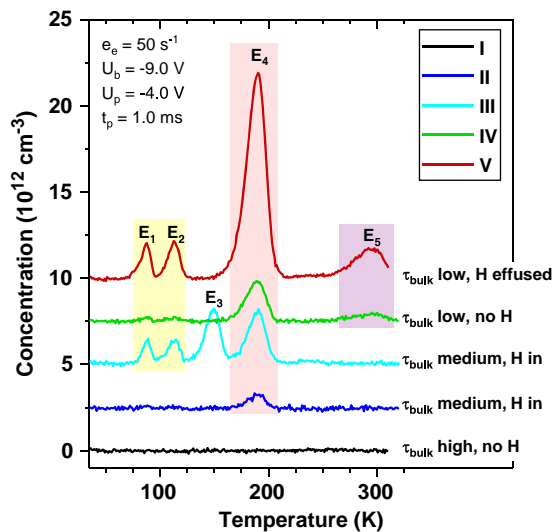


Figure 7. DLTS spectra converted into concentration values recorded on FZ-Si samples that were subjected to different annealing treatments with and without $\text{SiN}_x\text{:H}$ coating (for details see Table 3). The measurement settings (e_e : DLTS rate window, U_b : bias voltage, U_p : filling pulse voltage, t_p : filling pulse length) are shown in the graph. The spectra are offset vertically by $2.5 \times 10^{12} \text{ cm}^{-3}$ each for better visibility.

Table 3. Process details of the DLTS samples shown in Figure 7.

Process	I	II	III	IV	V
τ_{bulk} -degradation (RTA, 600 °C)	–	✓	–	✓	–
$\text{SiN}_x\text{:H}$ deposition (PECVD, 235 °C)	–	✓	✓	–	✓
Anneal with $\text{SiN}_x\text{:H}$ (TFA, 600 °C)	–	✓	✓	–	✓
Anneal bare/stripped wafer (TFA, 600 °C)	–	–	–	✓	✓

peak E_5 occurs (highlighted in purple), which is a very deep center with a corresponding electron activation energy of $0.645 \pm 0.007 \text{ eV}$. In contrast, DLTS peaks E_1 and E_2 (at $0.163 \pm 0.001 \text{ eV}$ and $0.198 \pm 0.002 \text{ eV}$, respectively; highlighted in yellow) do not appear to have a correlation with the bulk lifetime. These peaks could be features of shallow electron traps that do not notably contribute to electron-hole recombination. Surprisingly, these two peaks appear only for samples that were initially not τ_{bulk} -degraded by RTA, irrespective of the subsequent process steps.

In the framework of Shockley–Read–Hall (SRH) recombination, both parameters are important—the energetic position in the bandgap and the defect concentration. Furthermore, the capture cross-sections play a crucial role. Due to the exponential energy term, the energy difference of E_5 versus E_4 allows for an about two orders of magnitude higher recombination rate per defect (under the assumption of equal capture cross-sections). DLTS peaks E_4 range from trap concentrations of $\approx 1 \times 10^{12} \text{ cm}^{-3}$ (II) to $\approx 12 \times 10^{12} \text{ cm}^{-3}$ (V) and these traps are, if at all, only partially passivated by hydrogen. However, DLTS peaks E_5 have concentrations of $\approx 6 \times 10^{11} \text{ cm}^{-3}$ (IV) to $\approx 16 \times 10^{11} \text{ cm}^{-3}$ (V), but this trap is completely absent for the hydrogenated samples (II, III), which identifies the root cause of the intermediate τ_{bulk} -levels upon hydrogenation. Due to its near-midgap position, defect E_5 is highly recombination active and even small concentrations (10^{11} cm^{-3} range) lead immediately to low bulk lifetimes, whereas defect E_4 is less recombination active so that concentrations of up to $\approx 3 \times 10^{12} \text{ cm}^{-3}$ (III) still allow for an intermediate τ_{bulk} .

3. Discussion

3.1. Density Functional Theory

In the following, two recombination-active defects will be considered to discuss the possible evolution with thermal processing, i.e., formation and activation of the defects, their annihilation, and the apparent H-passivation. It is assumed that N is a constituent of these defects as its absence (N-lean FZ-Si) suppresses thermally induced τ_{bulk} -degradation.^[11] For the transport of N in Si in the temperature window used here, activation energies of $2.8^{[32]}$ to $3.24 \pm 0.25 \text{ eV}^{[33]}$ were reported. These values show a striking coincidence with the activation energy of the defect annihilation of $3.1 \pm 1.0 \text{ eV}$ (Arrhenius plot in Figure 4a), although that data analysis should be treated with caution as explained earlier. In ref. [34], it was shown that the effusion of N sets in rather spontaneously between 800 and 900 °C, in accordance with the recovery of τ_{bulk} (cf. Figure 3 and 4). It is

therefore postulated that defect annihilation starts with the spontaneous dissociation (decomposition) of the V_xN_y centers and subsequent N-effusion (time dependent). Hence, these τ_{bulk} -degrading defects can be deactivated on short timescales if the required thermal energy is provided. This effect is independent from the complete N-effusion from the wafer, which explains the measurable presence of N after 1 min, 900 °C RTA despite of a very high τ_{bulk} . Conversely, the presence of residual N after a short high-temperature annealing bears the chance for the reformation of V_xN_y centers during a subsequent medium-temperature annealing (cf. Figure 3b).

What are the possible V_xN_y configurations? N_2 -dimer configurations are generally not considered to be electrically active defects.^[35,36] The absence of states in the Si-bandgap is consistent with our own DFT calculations on extended approximants emulating the bulk phase ($Si_{453}N_2H_{196}$, not shown) and contradicts the assumption that V_2N_2 causes the τ_{bulk} -degradation.^[37,38] In contrast, in a V_1N_1 center, a substitutional trivalent N-atom occupies a tetravalent Si-vacancy, which creates a Si dangling bond (DB) defect. According to DFT, this defect has occupied and unoccupied states in the Si-bandgap, which—extrapolated to the bulk—are located at ≈ 0.2 eV from either of the band edges, as shown in Figure 8. Our DFT calculations showed further that a saturation of this Si-DB with H removes the defect level from the fundamental gap ($Si_{454}HNH_{196}$, not shown). The energetic position of $E_C - 0.2$ eV does not fully match with the electron activation energy of DLTS-peak E_4 (0.336 ± 0.003 eV), but still these two could be connected. In contrast, VN_3 species (N-trimers)

were proposed by Voronkov and Falster^[36] to be deep donors at $E_V + 0.46$ eV (corresponding to $E_C - 0.66$ eV), which coincides with the electron activation energy of DLTS-peak E_5 (0.645 ± 0.007 eV).

Aside from the basic defect constituents V and N, it is also important to keep in mind that other light impurities such as C and O are present with sufficient abundance (>ppb concentrations) to become involved in complexes that create DB defects. DFT calculations are in progress to identify possible candidates.

Considering the V_1N_1 center with its Si-DB defect, two more experimental observations can be consistently explained. First, in Section 2.5, a defect formation energy of 2.0 ± 0.3 eV was derived from Arrhenius plots (subject to future confirmation), which resembles the activation energy of 1.9 eV for H-depassivation of defects at the Si/SiO₂ interface capped with ALD-Ga₂O₃ as H-source.^[39] For RTA, which involves a high density of light-induced free carriers, a defect formation energy of only 1.2 ± 0.1 eV was fitted, which is similar to the situation of H-bonds in amorphous Si: The dissociation energy of Si-H is significantly reduced in the presence of light-induced carriers.^[40,41] Hence, the thermal activation of the τ_{bulk} -degradation appears to be (at least in part) related to the dissociation of Si-H bonds that initially passivate the Si-DBs opposing the V_1N_1 center. This explains why FZ-Si wafers have high bulk lifetimes in their as-fabricated out-of-box state. We postulate that the initial H-passivation occurs during cool down of the FZ-Si ingot by hydrogen trace impurities in the process gasses (Ar, N₂). Moreover, this Si-DB defect can also be efficiently repassivated with H by providing a H-source such as PECVD-SiN_x:H or ALD-Al₂O₃ during annealing.

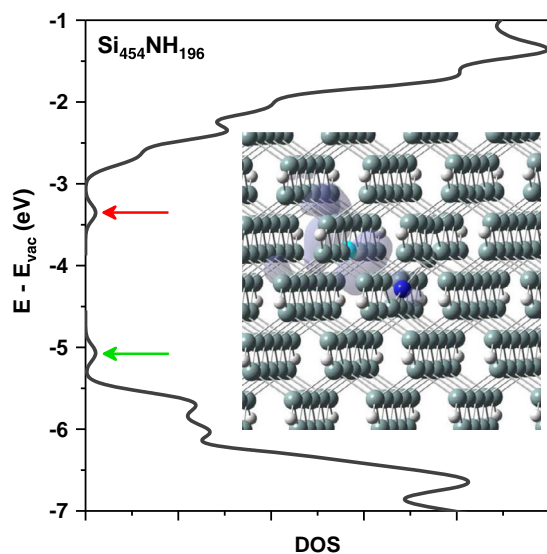


Figure 8. Density of states (DOS) calculated by DFT simulations of a $Si_{454}NH_{196}$ approximant (2.59 nm in size, zoomed central region shown in the inset) with a V_1N_1 defect, i.e., a single substitutional N-atom (dark blue) in a Si-vacancy and an opposing Si-atom (cyan) with a DB defect (other Si-atoms gray, surface terminating H-atoms white). The defect causes two states in the Si bandgap, an unoccupied state (indicated by the red arrow) and an occupied state (indicated by the green arrow). Extrapolated to bulk-Si, these states are located 0.2 eV below the conduction band edge and 0.2 eV above valence band edge. The inset also shows the isodensity plot of the lowest unoccupied molecular orbital (LUMO, corresponding to red arrow in DOS).

3.2. Possible Defect Mechanisms

Based on experimental evidence from lifetime measurements, SIMS, DLTS, and DFT simulation results, we propose a model based on (at least) two different defect species causing the thermally induced τ_{bulk} -degradation in FZ-Si. Three features can be deduced for the first defect type: 1) It is configured as V_1N_1 complex, i.e., a N-atom substituting a Si-vacancy, which creates a Si-DB. After fabrication of the FZ-Si ingot, during cool down, these DBs are passivated by trace impurities of H in the process gasses, which inactivate the defects in the as-fabricated state. 2) During the first annealing of the wafer the Si-H bond dissociates. This process requires a thermal formation energy of ≈ 2 eV; enhancement by a high free-carrier density induced by light (RTA) diminishes the thermal formation energy to ≈ 1.2 eV. The unpassivated Si-DB is an active recombination center with states in the Si bandgap (≈ 0.2 eV from the band edge according to DFT). If high H-concentrations are provided during the annealing (from dielectric coatings), the Si-DBs can be constantly repassivated in a dynamic equilibrium, which practically deactivates this defect type on a temporary basis. 3) For temperatures in excess of 800 °C, the V_1N_1 complex dissociates (binding energy ≈ 3.1 eV), which instantaneously annihilates the defect center. However, the complete effusion of N over the whole thickness of the wafer requires time. For short high-temperature anneals, a detectable amount of N is left behind and capable to

reconstitute some V_1N_1 defects during a subsequent medium-temperature treatment. Hence, a complete defect annihilation requires time to effuse all nitrogen.

For the second defect type, less information is available. It is most likely related to a nitrogen-vacancy center but could also involve other impurity elements. The activation of the second defect species appears to be indistinguishable from the first as no stepwise or gradual τ_{bulk} -degradation as a function of either temperature or time was observed. In contrast, the degradation is similar to a digital on/off process. Also, the annihilation behavior of the second defect type cannot be separated from the first in the lifetime data. However, the inefficiency or even absence of hydrogenation is characteristic for this defect. Even a massive supply of H does not efficiently inactivate the second defect type, as featured for instance by DLTS peak E₄. Yet, it is too early to identify this DLTS peak with the second defect type (and correspondingly DLTS peak E₅ with the first defect type). More DFT data are required as well as a correlation of the DLTS data with the hole-capturing properties of the observed defects.

We note that generally just a fraction of the available N (here $\approx 5 \times 10^{14} \text{ cm}^{-3}$) is required to form the V_1N_1 and other defects, which are expected to have concentrations in the range of 10^{12} – 10^{13} cm^{-3} . A majority of N will be configured as electrically inactive dimers.^[35,36]

4. Conclusion

The thermal bulk lifetime degradation and recovery of FZ–Si was studied by SA passivation using different annealing technologies (TFA, RTA, FLA) covering more than five orders of magnitude in dwell time and temperatures up to the melting point of Si. We showed that for as-cut and saw-damage etched wafers, various chemical pretreatments allow for excellent surface passivation by TFSI dissolved in hexane. In the critical temperature range from ≈ 300 – 800°C , there is no practical chance to avoid τ_{bulk} -degradation by shortening the annealing time. Even annealing dwell times on the sub-second time scale lead to τ_{bulk} -degradation. On the bright side, we demonstrated that the recovery of τ_{bulk} does not necessarily require long 1050°C anneals. 1 h tube furnace anneals at 900°C , or alternatively, minute-long RTA at this temperature, appear to be sufficient for a complete defect annihilation. In addition to the lower thermal budgets and a reduced contamination risk, such a process might allow for an in situ annihilation during, e.g., poly-Si crystallization anneals for passivating contacts. The onset of both τ_{bulk} -degradation and τ_{bulk} -recovery is very abrupt and can occur within temperature intervals of less than 17°C , whereby the defect formation occurs spontaneously. The complete and irreversible defect annihilation requires longer anneals. Hydrogen from H-rich dielectric coatings was shown to provide for a partial and only temporary stabilization of τ_{bulk} , approximately one order of magnitude above the fully degraded state ($\approx 40 \mu\text{s}$) but by far not near the initial or fully annihilated state (up to $\approx 8 \text{ ms}$). Hydrogenation of the FZ-inherent bulk defects is therefore not considered as a viable or reliable strategy to stabilize τ_{bulk} against thermal degradation.

5. Experimental Section

Sample Preparation: As-cut and initially $300 \mu\text{m}$ thick FZ–Si wafers, 100 mm in diameter, $\langle 100 \rangle$ -oriented, n-type (P) with $2.0 \Omega \text{ cm}$ resistivity, were RCA-cleaned and saw-damaged in 25%–TMAH at $\approx 80^\circ\text{C}$ to remove $\approx 10 \mu\text{m}$ Si per side. The wafers were cleaved into quarters and RCA-cleaned directly before thermal processing. Annealing in tube furnaces was carried out under a constant O_2 or N_2 gas flow of $\approx 200 \text{ l h}^{-1}$. For high temperatures, heating/cooling ramps of $\approx 20 \text{ K min}^{-1}$ from/to the loading/unloading temperature of 700°C were used. Before processing each batch of samples, the furnaces were cleaned by TLC and O_2 at 1100°C . All temperatures refer to the setpoint values, which were calibrated by a thermocouple probe. Errors of $\pm 3^\circ\text{C}$ are expected. For RTA, a UniTemp UTP-1100 system with a quartz glass chamber was used with a constant O_2 or N_2 gas flow of $\approx 600 \text{ l h}^{-1}$ and quartz glass pins to support the samples. The RTA-thermocouple did not touch an actual sample but a clean dummy from the same wafer material to avoid potential metal contamination. FLA was performed for 20 ms in oxygen ambient using continuous flow of O_2 . The FLA system was composed of 12 Xe lamps, 28 cm long. It allows for homogeneous annealing of 100 mm wafers using a single flash pulse. The energy density deposited to the sample surface during a single flash pulse was in the range of 33.5 – 126.0 J cm^{-2} . An annealing step of about 100°C difference was achieved by an energy density increase of about 10 J cm^{-2} . The annealing of a Si wafer with the lowest energy density (33.5 J cm^{-2}) allowed to achieve about 600°C , whereas annealing with 122.0 J cm^{-2} heated the Si up to a temperature of about 1300°C . Annealing with an energy density of 126 J cm^{-2} led to the melting of Si surface. The heating rate during 20 ms annealing was on the order of 100 K ms^{-1} , whereas the cooling rate was on the order of 200 K s^{-1} . ALD– Al_2O_3 layers were deposited in a Beneq TFS 200 system by 200 cycles of trimethylaluminum (TMAI) and water at 200°C . PECVD– SiN_x :H thin films were deposited in a Roth & Rau AK400 system at $\approx 235^\circ\text{C}$ using SiH_4 , NH_3 , and Ar. The 105 nm thick films (according to ellipsometry) had a density of $1.03 \times 10^{17} \text{ at cm}^{-2}$ with a SiN_x -stoichiometry of $x = 1.376$ and the following impurities: $[\text{H}] = 20.5 \text{ at\%}$, $[\text{C}] = 0.6 \text{ at\%}$, $[\text{O}] = 2.5 \text{ at\%}$, $[\text{F}] = 0.4$ – 0.7 at\% , $[\text{Ar}] = 0.5 \text{ at\%}$ (according to ERDA). Neither the ALD nor the PECVD dielectric thin films were subjected to any additional annealing to activate the surface passivation; just the thermal processes indicated in the text and figures were done.

Before SA passivation, all dielectric layers (SiO_2 , Al_2O_3 , SiN_x) were stripped by HF, etched in TMAH (25%, $\approx 80^\circ\text{C}$, 10 min), dipped in a HF/HCl solution ($\approx 1\%$), RCA-2 cleaned (10 min), and immersed in HF/HCl solution ($\approx 1\%$) for at least 1 min. Without deionized (DI)-water rinsing, the samples were pulled dry and immersed directly for $\approx 30 \text{ s}$ in the SA solution of 2 mg ml^{-1} TFSI in *n*-hexane (which was mixed in a N_2 -glovebox). The samples were then allowed to dry in ambient air in a fume hood and soon after lifetime measured.

Measurements: The effective minority carrier lifetimes τ_{eff} were measured using a Sinton Instruments WCT-120 photoconductance tool. The measured τ_{eff} from SA-passivated samples is identified with τ_{bulk} without further correction for residual surface recombination, as typical measured surface saturation current densities $J_{0,s}$ are in the range of $< 5 \text{ fA cm}^{-2}$ and the parameterized surface recombination velocity^[16] for our material is $S_{\text{eff}} \approx 0.99 \pm 0.04 \text{ cm s}^{-1}$. Uncalibrated PL lifetime images were obtained using a BT Imaging LIS-R1 system with an illumination level of 0.87 suns and 0.1 s exposure time for all samples. ERDA measurements were performed with a Bragg ionization chamber using a $43 \text{ MeV } ^{35}\text{Cl}^{7+}$ beam. A separate silicon detector with a Kapton absorber foil was used to detect hydrogen recoils and a sample with a known H concentration was used to verify the hydrogen quantification. Dynamic SIMS in negative polarity was measured using a Cameca IMS-4f with 14.5 keV Cs^+ primary ions with various current densities. The analyzed area had a diameter of $33 \mu\text{m}$ and depth at which N was quantified ranged from ≈ 5 to $25 \mu\text{m}$. Each SIMS measurement was repeated twice or thrice for increased accuracy. Circular Schottky barrier diodes (SBDs) of 1 mm diameter were formed on the cleaned surface of the samples using thermal evaporation of Au through a shadow mask, whereas a layer of Al was

thermally evaporated onto the back surface to create an ohmic contact. The diodes were characterized using capacitance–voltage and current–voltage measurements, and the highest quality diodes were chosen for conventional and high-resolution Laplace DLTS measurements.^[42]

DFT-Simulations: Hybrid density functional theory (h-DFT) calculations were carried out in real space with a molecular orbital basis set (MO-BS) and both Hartree–Fock (HF) and h-DFT methods as described later, using the Gaussian09 program suite.^[43] The MO-BS wavefunction ensemble was tested and optimized regarding the energy minimum of the approximant (variational principle) with the HF method using a 3-21 G MO-BS.^[44] Subsequently, structural optimization of the approximant to arrive at its most stable spatial configuration was carried out. Using these optimized geometries, their electronic structure was calculated again by testing and optimizing the MO-BS wavefunction ensemble with the B3LYP hybrid DF^[45,46] and the 6-31 G(d) MO-BS^[47] (B3LYP/6-31 G(d)). More details and extensive accurate evaluations can be found elsewhere.^[48–51] Approximants and MOs were visualized with Gview5.^[52]

Acknowledgements

D.H. thanks the Alexander von Humboldt Foundation for a Feodor Lynen Fellowship and acknowledges funding by the Australian Centre for Advanced Photovoltaics (ACAP, Collaboration Grant). Work at the University of Manchester was supported by EPSRC (grants EP/M024911/1 and EP/TO25131/1). D.K. acknowledges use of the Abacus compute cluster, IMDC, UNSW, funding by the 2015 UNSW Blue Sky Research Grant and by the 2018 Theodore-von-Kármán Fellowship of RWTH Aachen University, Germany. Work at the University of Warwick was supported by EPSRC (grant EP/M024911/1).

Conflict of Interest

The authors declare no conflict of interest.

Keywords

bulk lifetime, defects, float-zone silicon, nitrogen vacancy centers, photovoltaics

Received: July 8, 2020

Revised: July 20, 2020

Published online: August 6, 2020

- [1] J. Schmidt, K. Bothe, *Phys. Rev. B* **2004**, 69, 024107.
- [2] W. P. Mulligan, D. H. Rose, M. J. Cudzinovic, D. M. De Ceuster, K. R. McIntosh, D. D. Smith, R. M. Swanson, *Proc. 19th EU PVSEC*, Paris **2004**, p. 387.
- [3] J. Vedde, T. Clausen, L. Jensen, *Proc. 3rd IEEE-WCPEC*, Osaka **2003**, p. 943.
- [4] J. Vedde, L. Jensen, T. Larsen, T. Clausen, *Proc. 19th EU PVSEC*, Paris **2004**, p. 1075.
- [5] J. Ott, T. P. Pasanen, P. Repo, H. Seppänen, V. Vähänissi, H. Savin, *Phys. Status Solidi A* **2019**, 216, 1900309.
- [6] F. E. Rougieux, N. E. Grant, C. Barugkin, D. Macdonald, J. D. Murphy, *IEEE J. Photovolt.* **2015**, 5, 495.
- [7] N. E. Grant, V. P. Markevich, J. Mullins, A. R. Peaker, F. Rougieux, D. Macdonald, *Phys. Status Solidi RRL* **2016**, 10, 443.
- [8] N. E. Grant, V. P. Markevich, J. Mullins, A. R. Peaker, F. Rougieux, D. Macdonald, J. D. Murphy, *Phys. Status Solidi A* **2016**, 213, 2844.
- [9] Y. Zhu, F. Rougieux, N. Grant, J. Mullins, J. A. De Guzman, J. D. Murphy, V. P. Markevich, G. Coletti, A. R. Peaker, Z. Hameiri, *AIP Conf. Proc.* **2019**, 2147, 140014.
- [10] W. von Ammon, R. Hölzl, J. Virbulis, E. Dornberger, R. Schmolke, D. Gräf, *J. Cryst. Growth* **2001**, 226, 19.
- [11] J. Mullins, V. P. Markevich, M. Vaqueiro-Contreras, N. E. Grant, L. Jensen, J. Jablonski, J. D. Murphy, M. P. Halsall, A. R. Peaker, *J. Appl. Phys.* **2018**, 124, 035701.
- [12] T. Rahman, A. To, M. E. Pollard, N. E. Grant, J. Colwell, D. N. R. Payne, J. D. Murphy, D. M. Bagnall, B. Hoex, S. A. Boden, *Prog. Photovolt. Res. Appl.* **2018**, 26, 38.
- [13] T. Niewelt, R. Post, F. Schindler, W. Kwapil, M. C. Schubert, *AIP Conf. Proc.* **2019**, 2147, 140006.
- [14] K. C. Fong, T. C. Kho, W. S. Liang, T. K. Chong, M. Ernst, D. Walter, M. Stocks, E. Franklin, K. McIntosh, A. Blakers, *Sol. Energy Mater. Sol. Cells* **2018**, 186, 236.
- [15] T. Niewelt, A. Richter, T. C. Kho, N. E. Grant, R. S. Bonilla, B. Steinhauser, J. I. Polzin, F. Feldmann, M. Hermle, J. D. Murphy, S. P. Phang, W. Kwapil, M. C. Schubert, *Sol. Energy Mater. Sol. Cells* **2018**, 185, 252.
- [16] N. E. Grant, T. Niewelt, N. R. Wilson, E. C. Wheeler-Jones, J. Bullock, M. Al-Amin, M. C. Schubert, A. C. van Veen, A. Javey, J. D. Murphy, *IEEE J. Photovolt.* **2017**, 7, 1574.
- [17] J. Bullock, D. Kiriya, N. Grant, A. Azcatl, M. Hettick, T. Kho, P. Phang, H. C. Sio, D. Yan, D. Macdonald, M. A. Quevedo-Lopez, R. M. Wallace, A. Cuevas, A. Javey, *ACS Appl. Mater. Interfaces* **2016**, 8, 24205.
- [18] A. I. Pointon, N. E. Grant, E. C. Wheeler-Jones, P. P. Altermatt, J. D. Murphy, *Sol. Energy Mater. Sol. Cells* **2018**, 183, 164.
- [19] N. E. Grant, A. I. Pointon, R. Jefferies, D. Hiller, Y. Han, R. Beanland, M. Walker, J. D. Murphy, *Nanoscale* **2020**, <https://doi.org/10.1039/d0nr03860a>.
- [20] T. Niewelt, M. Selinger, N. E. Grant, W. Kwapil, J. D. Murphy, M. C. Schubert, *J. Appl. Phys.* **2017**, 121, 185702.
- [21] a) A. Richter, S. W. Glunz, F. Werner, J. Schmidt, A. Cuevas, *Phys. Rev. B* **2012**, 86, 165202; b) H. T. Nguyen, S. C. Baker-Finch, D. Macdonald, *Appl. Phys. Lett.* **2014**, 104, 112105.
- [22] L. Rebohle, S. Prucnal, W. Skorupa, *Semicond. Sci. Technol.* **2016**, 31, 103001.
- [23] U. Römer, R. Peibst, T. Ohrdes, B. Lim, J. Krügener, E. Bugiel, T. Wietler, R. Brendel, *Sol. Energy Mater. Sol. Cells* **2014**, 131, 85.
- [24] F. Feldmann, M. Simon, M. Bivour, C. Reichel, M. Hermle, S. W. Glunz, *Sol. Energy Mater. Sol. Cells* **2014**, 131, 100.
- [25] D. Yan, A. Cuevas, J. Bullock, Y. Wan, C. Samundsett, *Sol. Energy Mater. Sol. Cells* **2015**, 142, 75.
- [26] A. S. Kale, W. Nemeth, H. Guthrey, E. Kennedy, A. G. Norman, M. Page, M. Al-Jassim, D. L. Young, S. Agarwal, P. Stradins, *Appl. Phys. Lett.* **2019**, 114, 083902.
- [27] B. Steinhauser, J. I. Polzin, F. Feldmann, M. Hermle, S. W. Glunz, *Sol. RRL* **2018**, 2, 1800068.
- [28] S. E. Potts, W. Keuning, E. Langereis, G. Dingemans, M. C. M. van de Sanden, W. M. M. Kessels, *J. Electrochem. Soc.* **2010**, 157, P66.
- [29] O. M. E. Ylivaara, L. Kilpi, X. Liu, S. Sintonen, S. Ali, M. Laitinen, J. Julin, E. Haimi, T. Sajavaara, H. Lipsanen, S.-P. Hannula, H. Ronkainen, R. L. Puurunen, *J. Vac. Sci. Technol. A* **2017**, 35, 01B105.
- [30] D. Hiller, J. Göttlicher, R. Steininger, T. Huthwelker, J. Julin, F. Munnik, M. Wahl, W. Bock, B. Schoenaers, A. Stesmans, D. König, *ACS Appl. Mater. Interfaces* **2018**, 10, 30495.
- [31] H. Gnaser, *Appl. Phys. Lett.* **2001**, 79, 497.
- [32] T. Itoh, T. Abe, *Appl. Phys. Lett.* **1988**, 53, 39.
- [33] C. R. Alpass, J. D. Murphy, R. J. Falster, P. R. Wilshaw, *J. Appl. Phys.* **2009**, 105, 013519.

- [34] G. Mannino, V. Privitera, S. Scalese, S. Libertino, E. Napolitani, P. Pichler, N. E. B. Cowern, *Electrochem. Solid-State Lett.* **2004**, 7, G161.
- [35] R. Jones, S. Öberg, F. B. Rasmussen, B. B. Nielsen, *Phys. Rev. Lett.* **1994**, 72, 1882.
- [36] V. V. Voronkov, R. Falster, *J. Appl. Phys.* **2012**, 112, 013519.
- [37] N. Inoue, Y. Kawamura, *J. Appl. Phys.* **2018**, 123, 185701.
- [38] J. P. Goss, I. Hahn, R. Jones, P. R. Briddon, S. Öberg, *Phys. Rev. B* **2003**, 67, 045206.
- [39] T. G. Allen, A. Cuevas, *Appl. Phys. Lett.* **2014**, 105, 031601.
- [40] C. G. Van de Walle, R. A. Street, *Phys. Rev. B* **1994**, 49, 14766.
- [41] C. G. Van de Walle, R. A. Street, *Phys. Rev. B* **1995**, 51, 10615.
- [42] L. Dobaczewski, A. R. Peaker, K. Bonde Nielsen, *J. Appl. Phys.* **2004**, 96, 4689.
- [43] M. J. Frisch, G. W. Trucks, H. B. Schlegel, G. E. Scuseria, M. A. Robb, J. R. Cheeseman, G. Scalmani, V. Barone, G. A. Petersson, H. Nakatsuji, X. Li, M. Caricato, A. Marenich, J. Bloino, B. G. Janesko, R. Gomperts, B. Mennucci, H. P. Hratchian, J. V. Ortiz, A. F. Izmaylov, J. L. Sonnenberg, D. Williams-Young, F. Ding, F. Lipparini, F. Egidi, J. Goings, B. Peng, A. Petrone, T. Henderson, D. Ranasinghe, et al. *Gaussian09, Revision D.01*, Gaussian, Inc., Wallingford, CT, **2010**.
- [44] M. S. Gordon, J. S. Binkley, J. A. Pople, W. J. Pietro, W. J. Hehre, *J. Am. Chem. Soc.* **1982**, 104, 2797.
- [45] A. D. Becke, *Phys. Rev. A* **1988**, 38, 3098.
- [46] C. Lee, W. Yang, R. G. Parr, *Phys. Rev. B* **1988**, 37, 785.
- [47] M. M. Francl, W. J. Pietro, W. J. Hehre, *J. Chem. Phys.* **1982**, 77, 3654.
- [48] D. König, J. Rudd, M. A. Green, G. Conibeer, *Phys. Rev. B* **2008**, 78, 035339.
- [49] D. König, D. Hiller, S. Gutsch, M. Zacharias, *Adv. Mater. Interfaces* **2014**, 1, 1400359.
- [50] D. König, D. Hiller, N. Wilck, B. Berghoff, M. Müller, S. Thakur, G. Di Santo, L. Petaccia, J. Mayer, S. Smith, J. Knoch, *Beilstein J. Nanotech.* **2018**, 9, 2255.
- [51] D. König, N. Wilck, D. Hiller, B. Berghoff, A. Meledin, G. Di Santo, L. Petaccia, J. Mayer, S. Smith, J. Knoch, *Phys. Rev. Appl.* **2019**, 12, 054050.
- [52] R. Dennington, T. Keith, J. Millam, *GaussView 5.0.8*, Sernichem Inc., Shawnee Mission, KS, **2009**.